AGU PUBLICATIONS

Geophysical Research Letters

RESEARCH LETTER
10.1002/2015GL063695

Key Points:
- A spreading-aligned plate motion reference frame matches seismic anisotropy
- This defines a comprehensive reference frame matching hot spots
- Universal reference frame clarifies subduction zone trench migration

Supporting Information:
- Text S1 and Figures S1–S4

Correspondence to:
T. W. Becker,
twb@usc.edu

Citation:
Becker, T. W., A. J. Schaeffer, S. Lebedev, and C. P. Conrad (2015), Toward a generalized plate motion reference frame, *Geophys. Res. Lett.*, *42*, 3188–3196, doi:10.1002/2015GL063695.

Received 3 MAR 2015
Accepted 30 MAR 2015
Accepted article online 7 APR 2015
Published online 4 May 2015

Toward a generalized plate motion reference frame

T. W. Becker[1], A. J. Schaeffer[2], S. Lebedev[2], and C. P. Conrad[3]

[1]Department of Earth Sciences, University of Southern California, Los Angeles, Califonia, USA, [2]School of Cosmic Physics, Geophysics Section, Dublin Institute of Advanced Studies, Dublin, Ireland, [3]Department of Geology and Geophysics, SOEST, University of Hawai'i at Mānoa, Honolulu, Hawaii, USA

Abstract An absolute plate motion (APM) model is required to address issues such as the thermochemical evolution of Earth's mantle. All APM models have to rely on indirect inferences, including those based on hot spots and seismic anisotropy, each with their own set of uncertainties. Here, we explore a seafloor spreading-aligned reference frame. We show that this reference frame fits azimuthal seismic anisotropy in the uppermost mantle very well. The corresponding Euler pole is close to those of hot spot reference frames, ridge motion minimizing models, and geodynamic estimates of net rotation and predicts clear trench motion patterns. We conclude that a net rotation pole guided by the spreading-aligned model (at 64°E, 61°S, with moderate rotation of ∼ 0.2 … 0.3°/Myr) could indeed represent a standard, comprehensive reference frame for present-day plate motions with respect to the deep mantle.

1. Introduction

Any direct kinematic constraints on the motions of lithospheric plates, be they from geology or geodesy, can only yield relative velocity models, for example, with respect to slowly moving plates such as Africa. Any absolute reference frame requires additional assumptions, such as fixity of hot spots [*Morgan*, 1971] or other plate boundaries [*Kaula*, 1975]. Different assumptions lead to different absolute plate motion (APM) models, with important consequences, including for oceanic boundary layer dynamics (via seismic anisotropy) [*Becker*, 2001], subduction zone dynamics (via trench motions) [*Funiciello et al.*, 2008], or long-term Earth evolution (via thermochemical, top-down boundary layer interactions) [*Doubrovine et al.*, 2012]. It is therefore important to understand the implications of different APM models.

Hot spot reference frames can serve to illustrate some of the challenges in establishing APM models. In the simplest approach, the age progression of hot spot island chains is associated with strictly stationary plumes, anchored in the lower mantle, over which the lithosphere moves [*Morgan*, 1971]. It is indeed possible to construct global reference frames based on this assumption [*Minster and Jordan*, 1978], though the nature of those reference frames will depend on the geographic choice of hot spots [*O'Neill et al.*, 2005; *Morgan and Phipps Morgan*, 2007]. Selection of Pacific hot spots [*Gripp and Gordon*, 2002], for example, leads to APMs that have a larger amount of net rotation (NR) of the lithosphere with respect to the lower mantle than other choices. Moreover, plumes are not expected to be truly stationary. This can be explored in a predictive approach [*Steinberger and O'Connell*, 1998; *Boschi et al.*, 2008], and correction for relative plume motions leads to modified hot spot reference frames [*Steinberger et al.*, 2004].

A general way to distinguish between different APM models is to extract the net rotation compared to a plate motion model where this component is enforced to be zero, no-net-rotation (NNR) models. NR is defined as the degree one toroidal spherical harmonic component of plate motions, and lateral viscosity variations in the mantle are required for NR to exist [*O'Connell et al.*, 1991; *Ricard et al.*, 1991]. Possible candidates for such strength heterogeneities include subcontinental versus suboceanic plate asthenosphere viscosity differences [*Ricard et al.*, 1991; *Zhong*, 2001; *Becker*, 2006], likely combined with the stirring and driving effects of slabs [*Becker and Faccenna*, 2009; *O'Driscoll et al.*, 2009]. While typical geodynamic model predictions are on the low side of published net rotation rates [*Becker*, 2006; *Rudolph and Zhong*, 2014], large net rotations appear permissible within the uncertainties of mantle rheology [*Gérault et al.*, 2012; *Alisic et al.*, 2012].

This ambiguity motivates renewed efforts to understand the degree of net rotation and, more generally, to identify the most appropriate reference frame, at least for geologically recent (last few Myr) times where kinematic constraints on mantle dynamics are more complete [e.g., *Doubrovine et al.*, 2012]. In this context, seismic anisotropy may provide an important constraint, since most of the upper mantle anisotropy is expected to be

due to the lattice-preferred orientation (LPO) of intrinsically anisotropic olivine crystals in mantle flow [e.g., *Long and Becker*, 2010]. Azimuthal anisotropy is thus sensitive to the shearing expected in nonzero NR APM models throughout the upper ~500 km of the mantle [*Zhong* 2001; *Becker*, 2006].

Becker [2001] found that the addition of a large NR component to mantle circulation models of LPO alignment was incompatible with the fit to phase velocity maps of azimuthal anisotropy, suggesting a "speed limit" for net rotations. This argument was substantiated by *Conrad and Behn* [2010] using the match of mantle flow model predictions to *SKS* splitting and confirmed by *Becker et al.* [2014] for new surface wave models of azimuthal anisotropy.

Instead of comparing LPO estimates from actual mantle flow computations, one may also compare azimuthal anisotropy directly with the velocities from APM models [e.g., *Debayle and Ricard*, 2013; *Burgos et al.*, 2014]. This approach ignores the effect of return flow and density anomalies on scales smaller than the plates [e.g., *Long and Becker*, 2010] but might provide a first-order idea of the general sense of shear between plates and deeper mantle. *Kreemer* [2009] used this argument to invert *SKS* splitting orientations for a best fitting APM reference frame and discussed this model in light of hot spot motions, with an update and expanded error analysis provided by *Zheng et al.* [2014]. A fit of azimuthal anisotropy to an APM model was also used by *Montagner and Anderson* [2015] to infer plate motions for the Pacific, suggesting that the geographic distribution of misfits that can be derived from surface wave anisotropy might indicate the formation of a new plate boundary.

Given these different approaches to using azimuthal anisotropy in order to understand plate dynamics, *Becker et al.* [2014] tested mantle flow-derived LPO estimates and several APM-based models against seismic anisotropy. They found that LPO models provide the most consistent description of anisotropy and allow definition of a mechanical lithosphere in oceanic plates. However, *Becker et al.* [2014] also noted that the alignment of azimuthal anisotropy with APM models can be optimized by minimizing the average motions of spreading centers, suggesting the utility of a "ridge-no-rotation" (RNR) reference frame. This harks back to the earlier analysis of *Kaula* [1975] who explored holding various types of plate boundaries fixed.

Here we expand the range of evidence available to find a plausible and comprehensive global reference frame for present-day plate kinematics. We consider ridge proximal regions and show that a spreading-aligned reference frame conforms to various relevant constraints and fits diverse, independent data sets.

2. Results

Motivated by previous efforts on constraining APM models and the preliminary work by *Becker et al.* [2014] on a ridge-fixed reference frame, we set out to examine global plate kinematics and paleospreading orientations close to the current spreading centers. We use the plate boundary geometry of *Bird* [2003] and plate velocities in the NNR reference frame from MORVEL56-NNR [*Argus et al.*, 2011], the most recent and complete estimate of geologically "current" (i.e., last ~1 Ma, not geodetic) plate motions (Figure 1). However, other relative plate motion models such as NUVEL-1A [*DeMets et al.*, 1994] would lead to very similar results.

2.1. Spreading Alignment

We consider spreading orientations inferred from taking the gradient of *Müller et al.*'s [2008] seafloor age [cf. *Conrad and Lithgow-Bertelloni*, 2007], as used in a smoothed version by *Becker et al.* [2014]. Within a few Ma on each side of the spreading centers, those rates of spreading do not necessarily line up with relative plate motions in many published reference frames, for example, the NNR motions of MORVEL56 shown in blue vectors in Figure 1. Significant deviations are seen globally, in particular in the northern Atlantic and Indian Ocean basins.

Considering, alternatively, the alignment between paleospreading orientations and seismic anisotropy [e.g., *Debayle and Ricard*, 2013; *Becker et al.*, 2014], it is striking how well azimuthal anisotropy at asthenospheric depths, say at 150 km from the model of *Schaeffer and Lebedev* [2013a, 2013b], aligns with spreading [*Becker et al.*, 2014]. We therefore take the natural step of exploring if we can find a net rotation, expressed by an Euler vector $\boldsymbol{\omega}$, that minimizes the angular misfit, $\Delta\alpha$ ($\Delta\alpha \in [0; 90°]$ since orientations are 180° periodic), between plate velocities and spreading orientations, averaged over all of the samples along ridges shown in Figure 1, $\langle\Delta\alpha\rangle_r$. This hand-picked point set was constructed by visual inspection of seafloor ages and transform faults and attempts an even distance sampling at roughly constant age offset from the spreading centers. It will be compared with automatically created samples below.

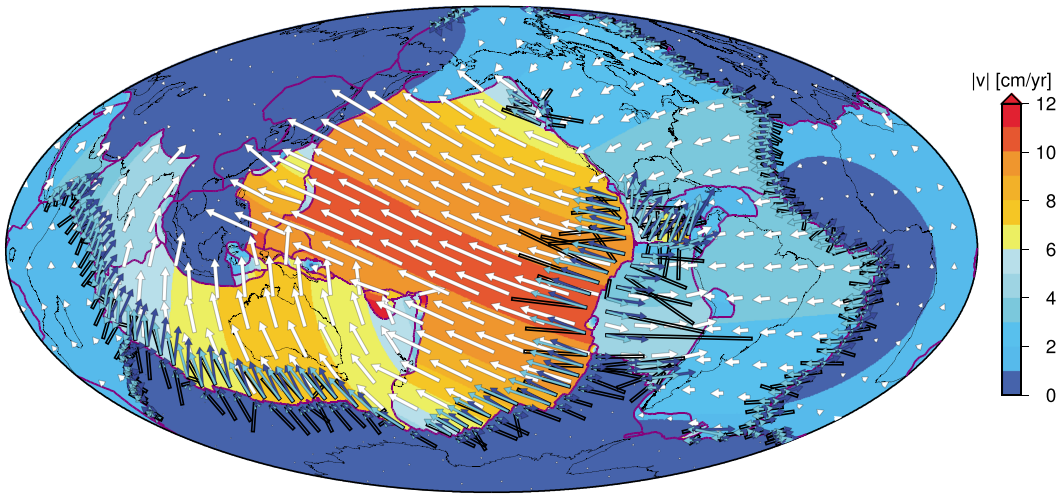

Figure 1. Global plate kinematics. Background colors and white arrows show magnitudes and directions of plate velocities in our preferred, spreading-aligned APM reference frame, respectively. Near the ridges, we compare paleospreading orientations (black sticks, computed by taking the gradient of *Müller et al.*'s [2008] seafloor age [cf. *Conrad and Lithgow-Bertelloni*, 2007]), with no-net-rotation reference frame MORVEL56 [*Argus et al.*, 2011] motions (blue vectors) and plate motions in our optimized, spreading-aligned reference frame (cyan vectors, see Table 1 and Figure 2). Ridge proximal sampling is based on hand-selected point pairs on each side of the spreading centers at constant age offset spacing; we show every sixth sample in this plot.

Optimization of $\langle\Delta\alpha\rangle_r$, like some of the other metrics we consider, is nonlinear, and we tested iterative (Levenberg-Marquardt) methods, but we prefer to complement a derivative-free, simplex minimization [*Nelder and Mead*, 1965] for the best Euler vector, $\boldsymbol{\omega}_{bf}$, with a fine parameter space exploration for constant rotation rate $|\boldsymbol{\omega}_{bf}|$, and in coarser increments for $|\boldsymbol{\omega}_{bf}| \in [0.05°/\text{Myr}; 0.8°/\text{Myr}]$ to check for robustness. This allows mapping out the geographic distribution of well-fitting Euler poles to get an idea of trade-offs and parameter uncertainties, which can be nontrivial (Figure S1 in the supporting information).

Table 1. Euler Poles With Respect to NNR-MORVEL56 [*Argus et al.*, 2011] and Misfit Metrics in Original and Best Fit Frames[a]

				Misfit ($\langle\Delta\alpha\rangle$ or $\langle\Delta v\rangle$)	
APM Model Type	Longitude (deg)	Latitude (deg)	Rate (°/Myr)	NNR Frame	APM Frame
Spreading alignment	63.9	−61.2	0.277	41.6°	26.4°
Ridge-no-motion	92.8	−35.5	0.167	2.5 cm/yr	1.9 cm/yr
Ridge-no-motion, rigid fit	98.1	−64.1	0.185		
SL2013SVA	53.7	−69.7	0.209	24.6°	16.5°
DR2012	63.1	−62.7	0.279	30.0°	21.2°
YB13	63.4	−62.7	0.271	24.8°	20.7°
SKS	158.9	−40.1	0.720	45.6°	28.2°
SKS-5	45.7	−45.2	0.252	34.9°	24.2°
MM07	79.4	−41.9	0.166	2.2 cm/yr	1.7 cm/yr
MM07-M	68.7	−41.9	0.207	2.6 cm/yr	2.0 cm/yr
Trench-no-motion	91.6	−1.9	0.200	3.0 cm/yr	2.6 cm/yr

[a] SL2013SVA, DR2012, and YB13 are based on azimuthal seismic anisotropy at 150 km depth from *Schaeffer and Lebedev* [2013a], *Debayle and Ricard* [2013], and *Yuan and Beghein* [2013], respectively, global oceanic mean angular misfit, $\langle\Delta\alpha\rangle_o$. *SKS* and *SKS-5* are based on optimizing the match with global *SKS* splitting and a 5° smoothed version thereof, respectively, $\langle\Delta\alpha\rangle_{SKS}$. MM07 is our fit of the *Morgan and Phipps Morgan* [2007] hot spot tracks, mean velocity misfit $\langle\Delta v\rangle_h$, MM07-M corrects for moving hot spots [*Doubrovine et al.*, 2012], $\langle\Delta v\rangle_{h-b}$, and "trench-no-motion" minimizes trench motions from *Heuret and Lallemand* [2005], $\langle\Delta v\rangle_t$ (cf. Figures 2 and S1).

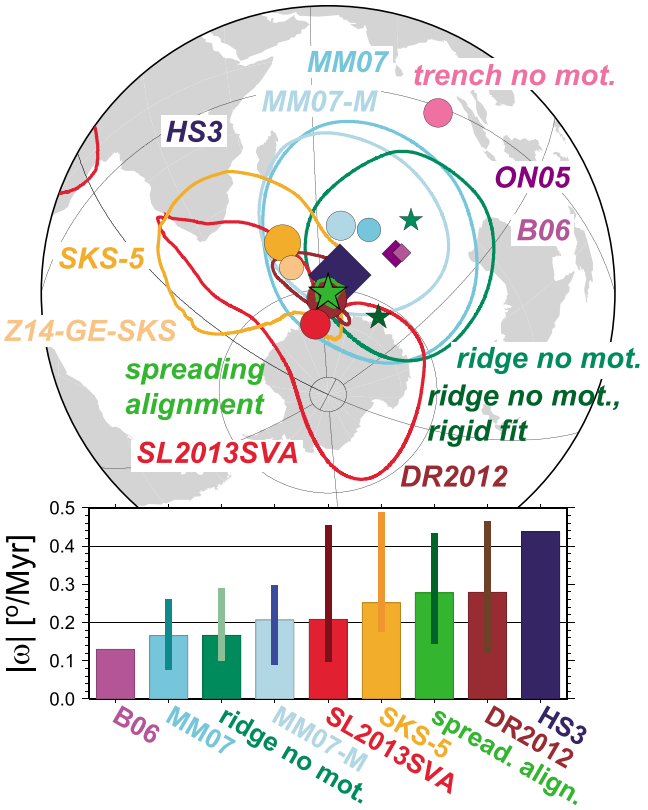

Figure 2. (top) APM model Euler pole locations and rates (symbol size) with respect to MORVEL56-NNR [*Argus et al.*, 2011] as in Table 1. Uncertainty contours for selected models show the range of pole locations within $\sigma_{\langle\Delta\alpha\rangle} = \langle\Delta\alpha\rangle_{\min} + 3°$ or $\sigma_{\langle\Delta v\rangle} = \langle\Delta v\rangle_{\min} + 2$ mm/yr of best solutions (cf. Figure S1). Hot spot models: HS3: *Gripp and Gordon* [2002] Pacific biased; MM07: fit of *Morgan and Phipps Morgan*, 2007's [2007] hot spot tracks; MM07-M: corrected for moving plumes [*Doubrovine et al.*, 2012]; ON05: *O'Neill et al.* [2005] Indo-African hot spots. B06: *Becker* [2006] convection model estimate of NR motion. Anisotropy match: *SKS-5*: based on 5° averaged *SKS* splitting; Z14-GE-*SKS*: global *SKS* reference frame from *Zheng et al.* [2014]; SL2013SV and DR2012: fit to azimuthal anisotropy at 150 km from *Schaeffer and Lebedev* [2013a] and *Debayle and Ricard* [2013], respectively (model by *Yuan and Beghein* [2013] has nearly identical pole to DR2012, Table 1). Spread.-align.: spreading-alignment reference frame; ridge no mot.: ridge-no-motion reference frames, minimizing all average motions and fitting a rigid motion to ridge pair velocities ("rigid fit"), respectively; trench no.-mot.: minimization of trench motions from *Heuret and Lallemand* [2005]. (bottom) Comparison of selected APM models in terms of their rotation rates (i.e., net rotation); vertical bars indicate range corresponding to $\sigma_{\langle\Delta\alpha\rangle}$ and $\sigma_{\langle\Delta v\rangle}$, respectively.

If we seek to optimize the global alignment of spreading orientations with plate motions using all of the points in Figure 1, we arrive at the best fitting Euler vector given in Table 1 (Figure 2). Mean angular misfits, $\langle\Delta\alpha\rangle_r$, are reduced dramatically from NNR values by this optimization, from 41.6° to 26.4° in the best fitting APM model (Figures 1 and S1). From visual inspection, it appears that this remaining misfit does mainly reflect the inherent small-scale variations of the spreading rates, at least partially due to uncertainties such as in the identification of magnetic lineations. We will compare misfit metrics for a variety of APM frames against those for NNR, noting that NNR is not necessarily a proper "reference" for $\langle\Delta\alpha\rangle_r$. Moreover, minimum misfits of different types of models cannot be directly compared quantitatively since they have different inherent "roughness."

Optimization of angular alignment leads to roughly small-circular regions of similar misfits for each ridge system considered (Figures S1b–S1d), but the global, spreading-alignment minimization surface makes the southern Indian Ocean Euler pole location well constrained (Figure 2). We have tested several ways of sampling ridges and weighting misfits. For example, we computed misfits based on all oceanic spreading center segments, excluding back-arc spreading, from *Bird* [2003], weighted by segment length, and then considered pair locations at 100 or 300 km distance orthogonal to each segment's azimuth. The resulting best fit Euler poles for spreading alignment are very close to the hand-picked sample-based inference (64°E, 61°S, 0.28°/Myr and 63°E, 62°S, 0.27°/Myr, respectively, cf. Table 1). Weighting the samples by spreading rate for

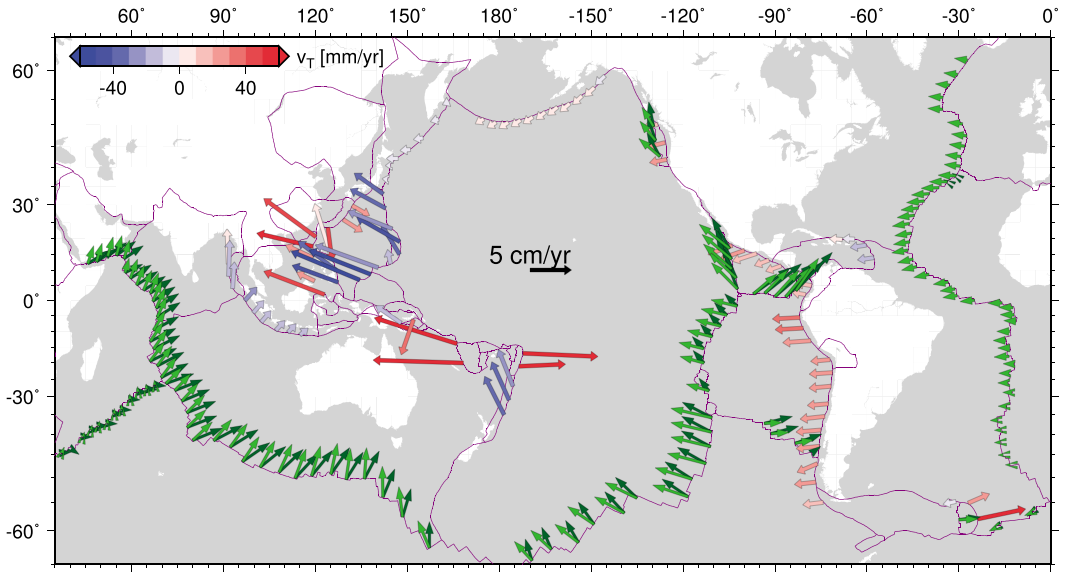

Figure 3. Trench motions from *Heuret and Lallemand* [2005] in our preferred, spreading-aligned reference frame (Figure 1) shown as blue-red vectors, colored by trench normal rates, v_T ($v_T > 0$ indicating trench rollback toward the subducting plate [cf., *Becker and Faccenna*, 2009]), plotted at every other sample. Mean spreading center motions shown at every sixth sample, for ridge-no-motion (dark green) and spreading-aligned (light green) reference frames. Only velocities larger than 5 mm/yr plotted.

the spreading-alignment optimization leads to a nearly identical pole for our hand-picked samples (64°E, 62°S, 0.27°/Myr). For the automatically generated samples, spreading rate weighting selects a northwestern Europe pole for 100 and 300 km distance pairs (6°W, 57°N, 0.34°/Myr and 2°W, 49°N, 0.29°/Myr, respectively), however. Those poles fall within the trade-off regions that can be seen in Figure S1a (i.e., geographic extent of low values of $\langle \Delta\alpha \rangle_r$), but we consider the Indian Ocean location of Figure 2 to be the more robust solution, since other choices for automated sampling poles, such as sample pairs that are offset by constant time (30 Myr) × spreading rate, prefer the Indian Ocean pole, even if weighted by spreading rate.

For comparison with *Becker et al.*'s [2014] RNR frame, we also recompute a ridge-no-motion reference frame using the samples of Figure 1 and fitting a single, best fit rotation pole to all ridge velocities by means of simple least squares. The resulting Euler pole assumes a rigid motion between ridges and is listed in Table 1 and compared to the spreading alignment and other poles in Figure 2. While similar in the style of motion (westward drift with Euler pole close to the South Pole at ~0.2°/Ma) and effect on the match to seismic anisotropy (see below) to the Euler pole of *Becker et al.* [2014], the locations are different by ~25°, due to different weighting, which is applied here more consistently.

If we use a global minimization of the mean motion of the pairs on each side of the ridges, $\langle \Delta v \rangle_r$, a modified ridge-no-rotation frame results, and the mean residual motion of all ridges defined in this way is $\langle \Delta v \rangle_r \approx 1.9$ cm/yr, not much reduced from $\langle \Delta v \rangle_r \approx 2.5$ cm/yr in the NNR reference frame. The Indian Ocean spreading ridge moves northward and the East Pacific Rise northwest even in this optimized frame, and only the Atlantic ridge system is approximately stationary (Figure 3). In contrast, the spreading-alignment optimization does orient spreading rates with plate motions overall (Figure 1). It is also in itself not unphysical, unlike the ridge-no-rotation reference frame, since spreading centers are not expected to be stationary in mantle convection.

2.2. Azimuthal Anisotropy

Plate motions need not be aligned with spreading orientations as defined here, either, but it is interesting to explore further what the spreading-aligned APM implies for the relative motions of plates and mantle. From *Becker et al.* [2014], we expect that an Euler pole close to the ridge-no-motion or spreading-aligned APM models will lead to a good match between APM models and azimuthal seismic anisotropy. Indeed, the global mean angular misfit in the oceanic plates, $\langle \Delta\alpha \rangle_o$, is quite small, 17.5°, for the spreading-alignment model compared to azimuthal anisotropy at 150 km depth (Figure S2), the lowest misfit depth as inferred by *Becker*

et al. [2014]. The misfit is 20.1° for ridge-no-rotation, similar to what was found by *Becker et al.* [2014] for their original RNR estimate.

We next compute an APM model that produces the best possible alignment of plate motions with azimuthal anisotropy from *Schaeffer and Lebedev* [2013a, 2013b] at 150 km depth, using equal area points sampling all of the oceanic plate regions, as in *Becker et al.* [2014], minimizing the mean misfit on those points, $\langle \Delta\alpha \rangle_o$. The best fitting Euler pole is very close to the spreading-aligned APM model (Table 1 and Figure 2), although there is a wide region of well-fitting Euler poles for seismic anisotropy alignment (roughly N-S band of low misfit in Figure S1f). The misfit surface for anisotropy, however, broadly resembles that of spreading alignment (Figure S1a). The mean global misfit between APM and anisotropy is small, $\langle \Delta\alpha \rangle_o \approx 16.2°$ (Figure S2); this compares to $\approx$ 21° for the models of *Debayle and Ricard* [2013] and *Yuan and Beghein* [2013] at the same depth (Figure S1). Their APM Euler poles are nearly identical, and both are close to the one based on *Schaeffer and Lebedev* [2013a] (Table 1 and Figure 2). Inspecting the geographical distribution of the misfit between azimuthal anisotropy and the corresponding best fit APM model (Figure S2), we find that the northern and southern parts of the Pacific plate are relatively less well matched compared to an equatorial band of near-perfect alignment, similar to what was discussed by *Montagner and Anderson* [2015]. This pattern is less clear when considering the model of *Debayle and Ricard* [2013] (Figure S3) but confirmed for anisotropy from *Yuan and Beghein* [2013] (Figure S4).

While the global average misfit of the spreading-aligned or anisotropy-optimized APM models is low compared to seismic anisotropy ($\langle \Delta\alpha \rangle_o \approx 17°$, Figure S2), asymmetric, large-scale misfit patterns, e.g., between the western and eastern Atlantic basin, remain for all seismological models considered (Figures S2–S4). In contrast, LPO from mantle flow shows large misfits mainly underneath spreading centers, which may be affected by partial melt and/or LPO reorientation, or in regions of intraplate deformation [*Becker et al.*, 2014], processes not captured well by simple flow models. LPO from mantle flow therefore appears to provide a tectonically simpler explanation for model misfit with azimuthal anisotropy. However, the detailed contributions of mantle flow and the geographic distribution of seismological model uncertainties remain to be fully understood, and it is clear that the spreading-aligned reference frame captures much of the signal in seismic anisotropy close to the spreading centers at asthenospheric depths. This implies that the shearing between plate and mantle that would be inferred from such APM models is an appropriate description of the major deformation style within the asthenosphere for young oceanic seafloor.

3. Discussion

From Figures 1 and 2, it is apparent that a spreading-aligned reference frame can be constructed with low misfits, and that the resulting APM model is very close (identical within parameter uncertainties) to the best fitting APM model defined by the orientational match to azimuthal anisotropy in the asthenosphere.

Complementing the analysis of *Zheng et al.* [2014], we also computed best fit APM models considering shear wave splitting using an update of the database of *Becker et al.* [2012] and trying to match APM motions to the station-averaged and smoothed "fast axes." We find that the station-averaged *SKS* splitting orientations can be fit only at $\langle \Delta\alpha \rangle_{SKS} \approx 28°$ (Figure S1), which appears in line with fairly large inherent variations of fast axes on small spatial scales [e.g., *Becker et al.*, 2012]. When *SKS* splits are averaged using a 5° spacing, mean angular misfit is reduced to $\approx 24°$, and the resulting APM model (Table 1) plots close to the estimate of *Zheng et al.* [2014] (Figure 2). Both *SKS* APM models fall within the range of APM models from azimuthal anisotropy at 150 km based on surface wave tomography (Figure 2) (see discussion in *Becker et al.* [2012]) and are, again, broadly consistent with the spreading-alignment Euler pole.

We next consider hot spot reference frame APM models. The Pacific hot spot-biased HS3 model of *Gripp and Gordon* [2002] is shown in Figure 2 alongside *O'Neill et al.*'s [2005] estimate and our newly computed hot spot reference frame based on *Morgan and Phipps Morgan* [2007]. This APM model was arrived at by adding a best fit net rotation to the NNR plate velocities so that all 33 hot spots with rate-defined tracks from *Morgan and Phipps Morgan*'s [2007] compilation are best matched (Figure S1 and Table 1).

We also corrected *Morgan and Phipps Morgan*'s [2007] tracks with the inferred plume conduit motions from *Doubrovine et al.* [2012], if available, resulting in 29 tracks. This assumption reduces the apparent net rotation that would be inferred from Pacific plate hot spots somewhat, since plumes there move mainly opposite to the Pacific plate, or net rotation, motion [*Steinberger et al.*, 2004]. However, globally, the moving plume pole

location is very similar to the stationary estimate (Figure 2), with slightly higher net rotation (Table 1) because of hot spots elsewhere on the globe. The effect of different weighting of hot spots given their geographic clustering remains to be explored.

Our APM model based on *Morgan and Phipps Morgan*'s [2007] tracks, for stationary or moving plumes, *O'Neill et al.*'s [2005] pole, and HS3 fall close to the spreading-alignment APM model (Figure 2). The figure also shows an estimate of net rotation induced by suboceanic/subcontinental asthenosphere viscosity differences from *Becker* [2006] (dislocation/diffusion creep rheology model). That geodynamic NR estimate falls, expectedly, in the vicinity of all previously discussed Euler poles, though the flow model predicts slower rotation rates. While the rotation rate for all of our best fit models (spreading alignment, anisotropy, and hot spots) is less well constrained than the location of the poles (i.e., the sense of net rotation motion), a rotation rate of $\sim 0.2 \ldots 0.3°$/Myr appears consistent with most models, and the spreading-aligned reference frame falls within the middle of the range of the amplitudes of westward motion (Figure 2). A spreading-aligned APM model at the lower end of the rotation rate uncertainty range is thus borderline consistent with the flow modeling-based constraints discussed by *Becker* [2001] and *Conrad and Behn* [2010].

These results suggest that there exists a generally valid reference frame for global plate motions. It can be constructed entirely kinematically by requiring spreading rates to align with plate motions, by means of inference from azimuthal anisotropy from both surface and body wave estimates, or by fitting hot spot tracks. Relative plate motions are, of course, expected to be spreading-center perpendicular, but absolute plate motions need not necessarily be aligned in this way. The finding that they are is consistent with the notion that ridges are passive features of plate tectonics. Relative and absolute plate motions in this view are set by other drivers, such as the global subduction system, and ridges passively respond. Having motions perpendicular to spreading centers is also consistent with the suggestion that transform faults are weak and so easily allow realignment of spreading centers during plate reorganizations.

This suggestion is borne out by geodynamic models to some extent. The sense of the net rotation of the spreading-aligned frame is consistent with what mantle flow models predict [*Zhong*, 2001; *Becker*, 2006], although some missing ingredient [*Gérault et al.*, 2012] apparently serves to speed net rotations up slightly beyond the rheological and structural effects considered by *Becker* [2006] (Figure 2). *Alisic et al.*'s [2012] models that include slabs in high resolution indeed indicate net rotations up to $\sim 0.2°$/Myr, as suggested by our spreading-aligned reference frame.

Considering the absolute plate velocities of this comprehensive, spreading-aligned reference frame (Figure 1), it is apparent that it also naturally leads to very slow motions of the Antarctic plate (mean velocities $\approx$ 3 mm/yr). Holding that plate fixed was suggested as a reference frame by *Hamilton* [2003], based on the observation that it is entirely surrounded by spreading centers. However, Eurasia is also moving quite slowly in our spreading-aligned reference frame ($\approx$ 5 mm/yr), for example, even though this plate abuts two subduction zones. This suggests that the type of plate boundary might not be a sufficient criterion for defining absolute motions.

Accepting that a reference frame with the spreading-alignment APM pole in Figure 2 in conjunction with a relative plate motion model such as MORVEL56-NNR [*Argus et al.*, 2011] provides a comprehensive description of the absolute motions of plates at present, we can consider the implications beyond the motions of hot spots or seismic anisotropy. *Funiciello et al.* [2008] explored how the strength of slabs determines their dynamics, including advance and rollback of the trench in response to slab bending and ponding. Estimates of actual trench motions in nature depend on the plate motion reference frame, and the degree of rollback and advance therefore has implications for slab dynamics, with large differences between NNR and the HS3, for example (also see discussion in *Becker and Faccenna* [2009]). This prompted *Schellart et al.* [2008] to further evaluate different hot spot reference frames in terms of their predictions for trench motions, leading them to favor the frame of *O'Neill et al.* [2005] based on a slab dynamics argument. *Williams et al.* [2015] evaluated the time dependence of the spread of trench retreat/advance statistics over the Cenozoic and explored if those can serve to constrain reference frames.

A strong degree of net rotation for the present day was invoked by *Doglioni et al.* [2007] in the context of subduction zone tectonics, and some net rotation does indeed seem to be required to explain deep slab stress states [*Carminati and Petricca*, 2010; *Alpert et al.*, 2010; *Alisic et al.*, 2012]. Given that both net rotation of the lithosphere and trench motions depend on the strength of slabs, we expect the two to be linked

[*Gérault et al.*, 2012; *Alisic et al.*, 2012]. It is therefore of interest to consider the implications of our preferred, spreading-aligned reference frame for subduction kinematics. Following *Kaula* [1975], we tried to minimize absolute trench motions (Table 1 and Figure 2), but remaining motions are quite large ($\langle \Delta v \rangle_t \approx 2.6$ cm/yr, computed on the samples shown in Figure 3) in this best fit frame, not much reduced from the original NNR mean motion, $\langle \Delta v \rangle_t \approx 3$ cm/yr. This indicates that, at least for the present-day plate tectonic setting, trench-no-motion reference frames are not easily achieved, just like ridge-no-motion, and exploring the systematics of motions statistics (i.e., deviations from the mean) may be a more meaningful exercise [*Williams et al.*, 2015].

Figure 3 shows trench motions from the compilation of *Heuret and Lallemand* [2005] for the present day in terms of trench rollback and advance using our preferred, spreading-aligned reference frame. It is striking how this APM model depicts all of the major eastern Pacific subduction zones as rolling back, more clearly distinguishing between different regions than other reference frames [cf. *Schellart et al.*, 2008; *Becker and Faccenna*, 2009]. Fast trench advance is predicted in regions with strong corner flow and pivoting (Tonga), continental plate interactions (Sumatra and Caribbean), and most clearly in an ocean-ocean setting, in the Philippine Sea Plate. There, double subduction, slab-slab interactions may explain the fast advance of the Marianas [*Carlson and Mortera-Gutiérrez*, 1990].

4. Conclusions

We show that optimizing the alignment of paleospreading orientations with plate motion leads to an absolute plate motion model that can be considered a comprehensive reference frame for present-day kinematics. This spreading-aligned APM model is consistent with predictions from mantle convection models and seismic anisotropy formation by shearing of the asthenosphere underneath lithospheric plates. The associated relative motions with respect to the deep mantle match those expected if plumes were the source of major hot spot volcanism. This provides a general framework for the interpretation of the evolution of subduction zones and long-term plate reorganizations.

Acknowledgments
We thank Caroline Beghein and Dietmar Mueller for their constructive assessments, Claudio Faccenna and Bernhard Steinberger for comments, and Bernhard for help with moving hot spots. All figures were created with the Generic Mapping Tools [*Wessel and Smith*, 1998]. T.W.B. was supported through NSF (EAR-1338329 and EAR-1215720), A.J.S. and S.L. were supported by Science Foundation Ireland (09/RFP/GEO2550 and 13/CDA/2192), and C.P.C. was supported through NSF EAR-1151241. All data sets and software used are available upon request.

The Editor thanks Dietmar Mueller and Caroline Beghein for their assistance in evaluating this paper.

References

Alisic, L., M. Gurnis, G. Stadler, C. Burstedde, and O. Ghattas (2012), Multi-scale dynamics and rheology of mantle flow with plates, *J. Geophys. Res.*, *117*, B10402, doi:10.1029/2012JB009234.

Alpert, L. A., T. W. Becker, and I. W. Bailey (2010), Global slab deformation and centroid moment constraints on viscosity, *Geochem. Geophys. Geosyst.*, *11*, Q12006, doi:10.1029/2010GC003301.

Argus, D. F., R. G. Gordon, and C. DeMets (2011), Geologically current motion of 56 plates relative to the no-net-rotation reference frame, *Geochem. Geophys. Geosyst.*, *12*, Q11001, doi:10.1029/2011GC003751.

Becker, T. W. (2006), On the effect of temperature and strain-rate dependent viscosity on global mantle flow, net rotation, and plate-driving forces, *Geophys. J. Int.*, *167*, 943–957.

Becker, T. W. (2008), Azimuthal seismic anisotropy constrains net rotation of the lithosphere, *Geophys. Res. Lett.*, *35*, L05303, doi:10.1029/2007GL032928. correction: doi:10.1029/2008GL033946.

Becker, T. W., and C. Faccenna (2009), A review of the role of subduction dynamics for regional and global plate motions, in *Subduction Zone Geodynamics*, edited by T. W. Becker and and C. Faccenna, pp. 3–34, Springer, Berlin.

Becker, T. W., S. Lebedev, and M. D. Long (2012), On the relationship between azimuthal anisotropy from shear wave splitting and surface wave tomography, *J. Geophys. Res.*, *117*, B01306, doi:10.1029/2011JB008705.

Becker, T. W., C. P. Conrad, A. J. Schaeffer, and S. Lebedev (2014), Origin of azimuthal seismic anisotropy in oceanic plates and mantle, *Earth Planet. Sci. Lett.*, *401*, 236–250.

Bird, P. (2003), An updated digital model of plate boundaries, *Geochem. Geophys. Geosyst.*, *4*(3), 1027, doi:10.1029/2001GC000252.

Boschi, L., T. W. Becker, and B. Steinberger (2008), On the statistical significance of correlations between synthetic mantle plumes and tomographic models, *Phys. Earth Planet. Inter.*, *167*, 230–238.

Burgos, G., J. -P. Montagner, E. Beucler, Y. Capdeville, A. Mocquet, and M. Drilleau (2014), Oceanic lithosphere/asthenosphere boundary from surface wave dispersion data, *J. Geophys. Res. Solid Earth*, *119*, 1079–1093, doi:10.1002/2013JB010528.

Carlson, R. L., and C. A. Mortera-Gutiérrez (1990), Subduction hinge migration along The Izu-Bonin-Mariana arc, *Tectonophysics*, *181*, 331–344.

Carminati, E., and P. Petricca (2010), State of stress in slabs as a function of large-scale plate kinematics, *Geochem. Geophys. Geosyst.*, *11*, Q04006, doi:10.1029/2009GC00303.

Conrad, C. P., and M. Behn (2010), Constraints on lithosphere net rotation and asthenospheric viscosity from global mantle flow models and seismic anisotropy, *Geochem. Geophys. Geosyst.*, *11*, Q05W05, doi:10.1029/2009GC002970.

Conrad, C. P., and C. Lithgow-Bertelloni (2007), Faster seafloor spreading and lithosphere production during the mid-Cenozoic, *Geology*, *35*, 29–32.

Debayle, E., and Y. Ricard (2013), Seismic observations of large-scale deformation at the bottom of fast-moving plates, *Earth Planet. Sci. Lett.*, *376*, 165–177.

DeMets, C., R. G. Gordon, D. F. Argus, and S. Stein (1994), Effect of recent revisions to the geomagnetic reversal time scale on estimates of current plate motions, *Geophys. Res. Lett.*, *21*, 2191–2194.

Doglioni, C., E. Carminati, M. Cuffaro, and D. Scrocca (2007), Subduction kinematics and dynamic constraints, *Earth Sci. Rev.*, *83*, 125–175.

Doubrovine, P. V., B. Steinberger, and T. H. Torsvik (2012), Absolute plate motions in a reference frame defined by moving hot spots in the Pacific, Atlantic, and Indian oceans, *J. Geophys. Res.*, *117*, B09101, doi:10.1029/2011JB009072.

Funiciello, F., C. Faccenna, A. Heuret, E. Di Giuseppe, S. Lallemand, and T. W. Becker (2008), Trench migration, net rotation and slab-mantle coupling, *Earth Planet. Sci. Lett.*, *271*, 233–240.
Gérault, M., T. W. Becker, B. J. P. Kaus, C. Faccenna, L. N. Moresi, and L. Husson (2012), The role of slabs and oceanic plate geometry for the net rotation of the lithosphere, trench motions, and slab return flow, *Geochem. Geophys. Geosyst.*, *13*, Q04001, doi:10.1029/2011GC003934.
Gripp, A. E., and R. G. Gordon (2002), Young tracks of hotspots and current plate velocities, *Geophys. J. Int.*, *150*, 321–361.
Hamilton, W. B. (2003), An alternative Earth, *Geol. Soc. Am.*, *13*, 4–12.
Heuret, A., and S. Lallemand (2005), Slab dynamics and back-arc deformation, *Phys. Earth Planet. Inter.*, *149*, 31–51.
Kaula, W. M. (1975), Absolute plate motions by boundary velocity minimization, *J. Geophys. Res.*, *80*, 244–248.
Kreemer, C. (2009), Absolute plate motions constrained by shear wave splitting orientations with implications for hot spot motions and mantle flow, *J. Geophys. Res.*, *114*, B10405, doi:10.1029/2009JB006416.
Long, M. D., and T. W. Becker (2010), Mantle dynamics and seismic anisotropy, *Earth Planet. Sci. Lett.*, *297*, 341–354.
Minster, J. B., and T. H. Jordan (1978), Present-day plate motions, *J. Geophys. Res.*, *83*, 5331–5354.
Montagner, J.-P., and D. L. Anderson (2015), The Pacific Megagash: A future plate boundary?, in *D. L. Anderson Honor Volume*, edited by G. R. Foulger, Geol. Soc. Am. [Available from http://www.mantleplumes.org/DLABook/Montagner_Accepted.pdf, accessed 01/2015.]
Morgan, J. P. (1971), Convection plumes in the lower mantle, *Nature*, *230*, 42–43.
Morgan, W. J., and J. Phipps Morgan (2007), Plate velocities in the hotspot reference frame, in *Plates, Plumes, and Planetary Processes, Special Papers*, vol. 430, edited by J. R. Foulger and and D. M. Jurdy, pp. 65–78, Geol. Soc. of Am., Boulder, Colo.
Müller, R. D., M. Sdrolias, C. Gaina, and W. R. Roest (2008), Age, spreading rates and spreading asymmetry of the world's ocean crust, *Geochem. Geophys. Geosyst.*, *9*, Q04006, doi:10.1029/2007GC001743.
Nelder, J. A., and R. Mead (1965), A simplex method for function minimization, *Comput. J.*, *7*, 308–313.
O'Connell, R. J., C. W. Gable, and B. H. Hager (1991), Toroidal-poloidal partitioning of lithospheric plate motions, in *Glacial Isostasy, Sea-Level and Mantle Rheology*, edited by R. Sabadini and and K. Lambeck, pp. 535–551, Kluwer Acad., Norwell, Mass.
O'Driscoll, L. J., E. D. Humphreys, and F. Saucier (2009), Subduction adjacent to deep continental roots: Enhanced negative pressure in the mantle wedge, mountain building and continental motion, *Earth Planet. Sci. Lett.*, *280*, 61–70.
O'Neill, C., D. Müller, and B. Steinberger (2005), On the uncertainties in hot spot reconstructions and the significance of moving hot spot reference frames, *Geochem. Geophys. Geosyst.*, *6*, Q0400, doi:10.1029/2004GC000784.
Ricard, Y., C. Doglioni, and R. Sabadini (1991), Differential rotation between lithosphere and mantle: A consequence of lateral mantle viscosity variations, *J. Geophys. Res.*, *96*, 8407–8415.
Rudolph, M. L., and S. J. Zhong (2014), History and dynamics of net rotation of the mantle and lithosphere, *Geochem. Geophys. Geosyst.*, *15*, 3645–3657, doi:10.1002/2014GC005457.
Schaeffer, A., and S. Lebedev (2013a), Global variations in azimuthal anisotropy of the Earth's upper mantle and crust, *Abstract DI11A-2172 presented at 2013 Fall Meeting, AGU*, San Francisco, Calif., 9–13 Dec.
Schaeffer, A., and S. Lebedev (2013b), Global shear speed structure of the upper mantle and transition zone, *Geophys. J. Int.*, *194*, 417–449.
Schellart, W. P., D. R. Stegman, and J. Freeman (2008), Global trench migration velocities and slab migration induced upper mantle volume fluxes: Constraints to find an Earth reference frame based on minimizing viscous dissipation, *Earth Sci. Rev.*, *88*, 118–144.
Steinberger, B., and R. J. O'Connell (1998), Advection of plumes in mantle flow: Implications for hotspot motion, mantle viscosity, and plume distribution, *Geophys. J. Int.*, *132*, 412–434.
Steinberger, B., R. Sutherland, and R. J. O'Connell (2004), Prediction of Emperor-Hawaii seamount locations from a revised model of global plate motion and mantle flow, *Nature*, *430*, 167–173.
Wessel, P., and W. H. F. Smith (1998), New, improved version of the Generic Mapping Tools released, *Eos Trans. AGU*, *79*, 579.
Williams, S., N. Flament, R. D. Müller, and N. Butterworth (2015), Absolute plate motions since 130 Ma constrained by subduction zone kinematics, *Earth Planet. Sci. Lett.*, *418*, 66–77.
Yuan, K., and C. Beghein (2013), Seismic anisotropy changes across upper mantle phase transitions, *Earth Planet. Sci. Lett.*, *374*, 132–144.
Zheng, L., R. G. Gordon, and C. Kreemer (2014), Absolute plate velocities from seismic anisotropy: Importance of correlated errors, *J. Geophys. Res.*, *119*, 7336–7352, doi:10.1002/2013JB010902.
Zhong, S. (2001), Role of ocean-continent contrast and continental keels on plate motion, net rotation of lithosphere, and the geoid, *J. Geophys. Res.*, *106*, 703–712.